 CMES, vol.103, no.3, pp.189-213, 2014

Vibration Control and Separation of a Device Scanning an Elastic Plate

Shueei-Muh Lin[1] **and Min-Jun Teng**[2]

Abstract: The control and separation of a scanning device moving along an arbitrary trajectory on an elastic plate is investigated. The system is a moving mass problem and is difficult to analyze directly. A semi-analytical method for the movingmass model is presented here. Without vibration control, the separation of a vehicle from a plate is likely to happen. The mechanism of separation of a vehicle from a plate is studied. Moreover, the effects of several parameters on vibration separation and the critical speed of system are studied. An effective control methodology is proposed for suppressing vibration and separation This model is applied to simulate a system containing a device scanning a plate. Due to the complexity of the moving-mass model, it is usually approximated by the moving-load model in most literature. The analytical solution of the moving-load model is also derived here and compared to the proposed models.

Keywords: movingmass model, plate, critical speed, separation, semi-analytical solution, vibration control.

Nomenclature

C	viscous damping of foundation
C_c	viscous damping of moving mass
c	dimensionless damping constant of foundation, $CL_1^2\sqrt{\rho h/D}$
c_c	dimensionless damping constant of moving mass, $C_cL_1\sqrt{\rho h/D}/L_2$
D	bending rigidity of plate, $Eh^3/[12(1-\mu^2)]$
E	Young's modulus
F_c	excitation force due to the moving mass
f_c	dimensionless excitation force due to the moving mass, $F_cL_1^3/D$

[1] Professor (corresponding author) of Mechanical Engineering Department, Kun Shan University, Tainan, Taiwan 710-03, Republic of China.

[2] graduate of Mechanical Engineering Department, Kun Shan University, Tainan, Taiwan 710-03, Republic of China.

g	acceleration of gravity
$\bar{g}$	ratio of weight and bending rigidity of plate, $\rho h L_1^3 g/D$
Gg	control parameter
h	thickness of plate
K	spring constant of the Winkler foundation
k	dimensionless spring constant of the Winkler foundation, KL_1^4/D
K_c	spring constant of moving mass
k_c	dimensionless spring constant of moving mass, $K_c L_1^3/DL_2$
L_1, L_2	lengths of the plate in the x- and y- directions, respectively
M_c	moving mass
m_c	mass ratio of moving mass and plate, $m_c = M_c/\rho h L_1 L_2$
r	aspect ratio, L_1/L_2
t	time variable
$v_{critical}$	dimensionless critical speed
W	transverse displacement of plate
W_c	transverse displacement of moving mass
w	dimensionless transverse displacements, W/L_1
w_c	dimensionless transverse displacements of moving mass, W_c/L_1
w_s	dimensionless static transverse displacements of plate
x, y, z	principal frame coordinates of plate
x_c, y_c, z_c	principal frame coordinates of moving mass
η_c	dimensionless principal frame coordinate of moving mass, z_c/L_1
μ	Poisson's ratio
ω_{mn}	natural frequency of plate
ξ, ζ	dimensionless principal frame coordinates of plate, $x/L_1, y/L_1$
ξ_c, ζ_c	dimensionless principal frame coordinates of moving mass, $x_c/L_1, y_c/L_1$
ζ_k	damping ratio
ρ	mass density
τ	dimensionless time, $t\sqrt{D/\rho h}/L_1^2$
∇^2	Laplace's operator

1 Introduction

The problem of moving mass has many engineering applications, most notably in the design of railroad tracks for high-speed train, roadways and airport runways for aircraft, bridges and elevated roadways for moving vehicles [Beskou and Theodorakopoulos, 2011], computer storage disk drives [Huang and Mote Jr., 1996] high speed precision machining [Esen, 2013] and the motion of moving beams [Lin, (2009a, 2009b, 2011)].

This problem is generally simulated using two models: (1) the moving-load model,

and (2) the moving-mass model. The major difference is that the inertial effects of the moving body are incorporated into the model formulations in the movingmass model, but not in the moving-load model Due to the complexity of the moving-mass model, the majority of studies available in the literature only consider the vertical translational component of the moving mass acceleration in the full term formulation of the problem, neglecting the other convective acceleration terms leading to error Akin and Mofid [1989] investigated a beam with moving mass and found that the moving-load model causes an error of 2∼80%. In addition, Nikkhoo *et al*. [2007] found for an Euler–Bernoulli beam, ignoring the convective terms in the formulation could lead to a remarkable error for mass velocities greater than a so-called critical velocity. Intuitively, for plate problems with more convective terms, this could be even more important.

In the moving-load model, Gbadeyan and Oni [1995] investigated the dynamic behavior of beams and rectangular plates under moving loads Huang and Thambiratnam [2001] investigated deflection response of plate on Winkler foundation in response to moving accelerated loads. Kim [2004] investigated the buckling and vibration of a plate on an elastic foundation subjected to in-plane compression and moving loads. Lee and Yhim [2004] investigated the dynamic response of composite plates subjected to multi-moving loads based on a third order theory. Moving velocities made greater contributions to the dynamic responses of the composite plates for higher speed. Moreover, the dynamic resistance for plates made of composite materials was excellent and stable. Wu [2005] proposed the approximated method predicting the dynamic responses of a two-dimensional rectangular plate undergoing a transverse moving line load by using the one-dimensional equivalent beam model. Au and Wang [2005] investigated sound radiation from forced vibration of rectangular orthotropic plates under moving loads. Based on the Rayleigh integral and the dynamic response of the plate, the acoustic pressure distributions around the plate were obtained in the time domain. Law et al. [2007] investigated the dynamic identification of moving loads from a vehicle traveling on top of a beam-slab type bridge deck using numerical and experimental studies. Elliott *et al.* [2007] described the location tracking of a moving load with an unknown, harmonically varying magnitude on a plate using a distributive sensing method. Using this method, the actual position of forces moving at various speeds can be determined to within 2% error at speeds less than 3.2 m/s. Malekzadeh *et al*. [2009, 2010] studied the dynamic response of thick laminated rectangular and annular sector plates subjected to moving load by using a three-dimensional hybrid numerical method. The hybrid method is composed of a series solution, layerwise theory and the differential quadrature method in conjunction with the finite difference method. Sheng and Wang [2011] investigated the response and control of functionally graded lami-

nated piezoelectric shells under thermal shock and movement loadings. They found that the maximum value of the displacement increases with increase in velocity of moving loads until a critical speed, and then decrease after this critical speed Zhang *et al*. [2011] proposed an approximate solution for the dual-duct simply supported rectangular plate subjected to a moving load using a stepped plate approximation theory. Martı'nez-Rodrigo and Museros [2011] studied the optimal design of passive viscous dampers for controlling the resonant response of orthotropic plates under high-speed moving loads. They found that for a particular set of auxiliary beams, there exist optimum parameters of passive viscous dampers that minimized the plate resonance.

In the moving-mass model, Gbadeyan and Dada [2006] took the finite difference method to solve the moving mass problem. Their study presented that the maximum shearing forces, bending and twisting moments occurred almost at the same time. Also, the values of the maximum deflections were higher for Mindlin plates than for non-Mindlin plates. Wu [2007] proposed the finite moving mass element method and studied the influence of moving-load-induced inertia force, Coriolis force and centrifugal force on the dynamic behavior of inclined plates subjected to moving loads. He concluded the effects of Coriolis force and centrifugal force were perceptible only in the case of higher moving-load speed. Rofooei and Nikkhoo [2009] derived the constitutive equation of motion for a thin rectangular plate with a number of piezo patches bonded on its surface under the excitation of a moving mass. Eigenfunction expansion was used to transform the equation of motion into a number of coupled ordinary differential equations. A classical closed-loop optimal control algorithm was employed to effectively suppress the resonant dynamic response of the system. Ghafoori and Asghari [2010] used the finite element method based on the first-order shear deformation theory and the Newmark direct integration method to study the dynamic behavior of composite plate Their research presented that the most sensitive lamination to the inertia of moving mass was [45/45/45/45] lamination so that the moving mass analysis gave poor results in the moving-load model Eftekhari and Jafari [2012] proposed the methodology composed of the Ritz method, differential quadrature method, integral quadrature method and Newmark time integration scheme to study the transient response of rectangular plates subjected to linearly varying inplane stresses and moving masses. Amiri *et al*. [2013] took into account the moving mass inertia effect all the convective terms of its out-of-plane acceleration components for the Mindlin plate. The eigenfunction expansion method transformed the governing equation into a set of ordinary differential equations and then solved by using the matrix-exponential based solution method. Their results showed, for moderately thick plates, there was the remarkable differences between the results in the Mindlin plate theory and

the classical plate theory. Esen [2013] used the finite element method to study the transverse vibration of rectangular thin plates under a moving mass. The literature presented that the vibration effect of the change in velocity was more significant when compared to the change in mass.

So far, little research has been devoted to the investigation of separation and vibration control of plate in the moving-mass model. This study is investigates the control and separation of a concentrated mass moving along an arbitrary trajectory on a plate. The semi-analytical solutions for these systems are presented. Moreover, the effects of several parameters on the separation and vibration control are investigated also.

2 Moving mass model

2.1 Governing Equation and Boundary Conditions

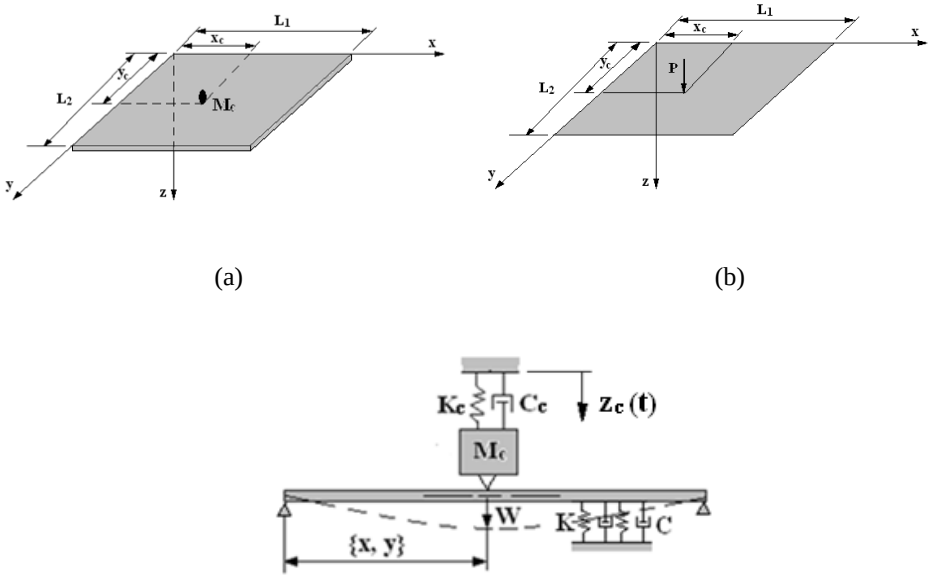

Figure 1: Geometry and coordinate system of a simply-supported plate subjected to a moving mass.

A concentrated mass moves along an arbitrary trajectory on a rectangular isotropic

elastic plate, as shown in Figure 1a. The governing equation is

$$D\nabla^4 W + C\frac{\partial W}{\partial t} + KW + \rho h\frac{\partial^2 W}{\partial t^2} = F_c\left(W_c, x_c, y_c, t\right) \tag{1}$$

The excitation forcing due to the moving mass is

$$F_c\left(x,y,t\right) = M_c\left(g - \frac{d^2 W_c\left(t\right)}{dt^2}\right)\delta\left(x - x_c\left(t\right)\right)\delta\left(y - y_c\left(t\right)\right) \tag{2}$$

Considering all the out-of-plane translational acceleration components of the moving mass, and observing the full contact condition between the moving mass and plate, Eq. (2) is expanded as:

$$\frac{d^2 W_c\left(t\right)}{dt^2} = \left[\begin{array}{l} \left(\frac{dx_c}{dt}\right)^2 \frac{\partial^2}{\partial x^2} + 2\frac{dx_c}{dt}\frac{dy_c}{dt}\frac{\partial^2}{\partial x \partial y} + 2\frac{dx_c}{dt}\frac{\partial^2}{\partial x \partial t} \\ + \left(\frac{dy_c}{dt}\right)^2 \frac{\partial^2}{\partial y^2} + 2\frac{dy_c}{dt}\frac{\partial^2}{\partial y \partial t} + \frac{d^2 x_c}{dt^2}\frac{\partial}{\partial x} + \frac{d^2 y_c}{dt^2}\frac{\partial}{\partial y} + \frac{\partial^2}{\partial t^2} \end{array}\right] W \tag{3}$$

The simply supported boundary conditions are

At y = 0:

$$W = 0 \tag{4}$$

$$\frac{\partial^2 W}{\partial y^2} + \mu\frac{\partial^2 W}{\partial x^2} = 0 \tag{5}$$

At $y = L_2$:

$$W = 0 \tag{6}$$

$$\frac{\partial^2 W}{\partial y^2} + \mu\frac{\partial^2 W}{\partial x^2} = 0 \tag{7}$$

At $x = 0$:

$$W = 0 \tag{8}$$

$$\frac{\partial^2 W}{\partial x^2} + \mu\frac{\partial^2 W}{\partial y^2} = 0 \tag{9}$$

At $x = L_1$:

$$W = 0 \tag{10}$$

$$\frac{\partial^2 W}{\partial x^2} + \mu\frac{\partial^2 W}{\partial y^2} = 0 \tag{11}$$

In terms of the dimensionless parameters in the nomenclature, the corresponding dimensionless governing equation is

$$\nabla^4 w + c\frac{\partial w}{\partial \tau} + kw + \frac{\partial^2 w}{\partial \tau^2} = f_c\left(w_c, \xi_c, \zeta_c, \tau\right) \tag{12a}$$

where

$$f_c\left(w_c, \xi_c, \zeta_c, \tau\right) = m_c\left(\bar{g} - \frac{d^2 w_c(\tau)}{d\tau^2}\right)\delta\left(\xi - \xi_c(\tau)\right)\delta\left(\zeta - \zeta_c(\tau)\right) \tag{12b}$$

and

$$\frac{d^2 w_c(\tau)}{d\tau^2} = \left[\begin{array}{l} \left(\frac{d\xi_c}{d\tau}\right)^2 \frac{\partial^2}{\partial \xi^2} + 2\frac{d\xi_c}{d\tau}\frac{d\zeta_c}{d\tau}\frac{\partial^2}{\partial \xi \partial \zeta} + 2\frac{d\xi_c}{d\tau}\frac{\partial^2}{\partial \xi \partial \tau} \\ + \left(\frac{d\zeta_c}{d\tau}\right)^2 \frac{\partial^2}{\partial \zeta^2} + 2\frac{d\zeta_c}{d\tau}\frac{\partial^2}{\partial \zeta \partial \tau} + \frac{d^2\xi_c}{d\tau^2}\frac{\partial}{\partial \xi} + \frac{d^2\zeta_c}{d\tau^2}\frac{\partial}{\partial \zeta} + \frac{\partial^2}{\partial \tau^2} \end{array}\right] w_c. \tag{12c}$$

The dimensionless boundary conditions are

At $\zeta = 0$:

$$w = 0 \tag{13}$$

$$\frac{\partial^2 w}{\partial \zeta^2} + \mu\frac{\partial^2 w}{\partial \xi^2} = 0 \tag{14}$$

At ζ =1/r:

$$w = 0 \tag{15}$$

$$\frac{\partial^2 w}{\partial \zeta^2} + \mu\frac{\partial^2 w}{\partial \xi^2} = 0 \tag{16}$$

The other two edges are also simply supported along the y direction:

At $\xi = 0$:

$$w = 0 \tag{17}$$

$$\frac{\partial^2 w}{\partial \xi^2} + \mu\frac{\partial^2 w}{\partial \zeta^2} = 0 \tag{18}$$

At $\xi = 1$:

$$w = 0 \tag{19}$$

$$\frac{\partial^2 w}{\partial \xi^2} + \mu\frac{\partial^2 w}{\partial \zeta^2} = 0 \tag{20}$$

2.2 Semi-analytical solution

From Eq. (12c) the absolute acceleration $d^2w_c/d\tau^2$ includes the Coriolis accelerations $\left\{2\frac{d\xi_c}{d\tau}\frac{\partial^2 w_c}{\partial\xi\partial\tau}, 2\frac{d\zeta_c}{d\tau}\frac{\partial^2 w_c}{\partial\zeta\partial\tau}\right\}$ and time-dependent coefficients$\{\xi_c(\tau), \zeta_c(\tau)\}$. Because the force f_c of Eq. (12b) includes the product of the unknown variable w_c and the time-dependent coefficients, this system composed of Eqs. (12)-(20) is implicit and very difficult to solve directly The semi-analytical methodology is presented. First, using the approximated acceleration method, the implicit system is transformed into an explicit system. Secondly, the analytical solution of the transformed system can be derived by using the mode superposition method. Finally, error due to transformation must be near zero. The details are demonstrated below

2.2.1 Approximated acceleration method

It is assumed that the overall dynamic behavior of the general system is composed of the behaviors of several time subintervals. The overall dynamic performance of the system is derived step by step. If each time subinterval $\Delta\tau$ is very small, the absolute acceleration can be linearly approximated as

$$\frac{d^2w_c}{d\tau^2} \approx \left[\frac{d^2w_c(\xi_c(\tau_i), \zeta_c(\tau_i), \tau_i)}{d\tau^2} + \lambda(\tau - \tau_i)\right] \triangleq \frac{d^2\bar{w}_c(\tau)}{d\tau^2}, \quad for \quad \tau_i < \tau < \tau_i + \Delta\tau = \tau_{i+1} \tag{21}$$

The approximated absolute acceleration is defined as $d^2\bar{w}_c/d\tau^2$ When the unknown parameter λ is correctly chosen the error of the acceleration at $\tau = \tau_{i+1}$ approaches zero, i.e.,

$$Error(\tau_{i+1}) = \left|\frac{d^2w_c(\tau_{i+1})}{d\tau^2} - \frac{d^2\bar{w}_c(\tau_{i+1})}{d\tau^2}\right| < \varepsilon \to 0. \tag{22}$$

It should be noted that if λ is correctly chosen the approximate acceleration $d^2\bar{w}_c(\tau_{i+1})/d\tau^2$ is calculated via Eq. (21). Substituting Eq. (21) into the governing equation (12), the transformed system is obtained:

$$\nabla^4 w + c\frac{\partial w}{\partial\tau} + kw + \frac{\partial^2 w}{\partial\tau^2} = \bar{f}_c(w_c, \xi_c, \zeta_c, \tau), \text{ for } \tau_i < \tau < \tau_{i+1} \tag{23}$$

where $\bar{f}_c(w_c, \xi_c, \zeta_c, \tau) = m_c\left(\bar{g} - d^2\bar{w}_c/d\tau^2\right)\delta(\xi - \xi_c)\delta(\zeta - \zeta_c)$

The implicit governing equation (12) becomes an explicit equation (23). Next, the analytical solution method is proposed and the absolute acceleration $d^2w_c(\tau_{i+1})/d\tau^2$ can be determined. By using the bisection method, an accurate value for parameter λ can be found to satisfy the minimum error condition (22).

2.2.2 Mode superposition method

The dynamic solution and the forcing term of Eq. (23) are respectively assumed to be

$$w = \sum_{m=1}^{\infty}\sum_{n=1}^{\infty} T_{mn}(\tau)\sin m\pi\xi \sin n\pi r\zeta, \tag{24a}$$

and

$$\bar{f}_c(\xi,\zeta,\tau) = \sum_{m=1}^{\infty}\sum_{n=1}^{\infty} \tilde{F}_{mn}(\tau)\sin m\pi\xi \sin n\pi r\zeta, \tag{24b}$$

where $\tilde{F}_{mn}(\tau) = 4m_c\left(\bar{g} - d^2\bar{w}_c/d\tau^2\right)\sin m\pi\xi_c \sin n\pi r\zeta_c$
Substituting Eq. (24) into the governing equation (23) obtains

$$\frac{d^2T_{mn}}{d\tau^2} + c\frac{dT_{mn}}{d\tau} + \left(\omega_{mn}^2 + k\right)T_{mn} = \tilde{F}_{mn}(\tau), \text{ for } \tau_i < \tau < \tau_{i+1}, \tag{25}$$

where $\omega_{mn}^2 = \left(m^4 + 2m^2(nr)^2 + (nr)^4\right)\pi^4$
Further, the solutions of Eq. (25) are derived as follows [34]:

$$\begin{aligned} T_{mn}(\tau) &= e^{-\zeta_k\omega_k(\tau-\tau_i)}\left[\cos\omega_{dk}(\tau-\tau_i) + \frac{\zeta_k\omega_k}{\omega_{dk}}\sin\omega_{dk}(\tau-\tau_i)\right]T_{mn}(\tau_i) \\ &+ \frac{1}{\omega_{dk}}e^{-\zeta_k\omega_k(\tau-\tau_i)}\sin\omega_{dk}(\tau-\tau_i)\frac{dT_{mn}(\tau_i)}{d\tau} \\ &+ \frac{1}{\omega_{dk}}\int_{\tau_i}^{\tau} e^{-\zeta_k\omega_k(\tau-\chi)}\sin\omega_{dk}(\tau-\chi)\tilde{F}_{mn}(\chi)d\chi, \end{aligned}$$

$$\begin{aligned} \frac{dT_{mn}(\tau)}{d\tau} &= -\left[\frac{(\zeta_k\omega_k)^2}{\omega_{dk}} + \omega_{dk}\right]e^{-\zeta_k\omega_k(\tau-\tau_i)}\sin\omega_{dk}(\tau-\tau_i)T_{mn}(\tau_i) \\ &+ \frac{1}{\omega_{dk}}e^{-\zeta_k\omega_k(\tau-\tau_i)}\left[\omega_{dk}\cos\omega_{dk}(\tau-\tau_i) - \zeta_k\omega_k\sin\omega_{dk}(\tau-\tau_i)\right]\frac{dT_{mn}(\tau_i)}{d\tau} \\ &+ \frac{1}{\omega_{dk}}\int_{\tau_i}^{\tau} e^{-\zeta_k\omega_k(\tau-\chi)}\left[\omega_{dk}\cos\omega_{dk}(\tau-\chi) - \zeta_k\omega_k\sin\omega_{dk}(\tau-\chi)\right]\tilde{F}_{mn}(\chi)d\chi, \end{aligned}$$

$$\begin{aligned}
&\frac{d^2T_{mn}(\tau)}{d\tau^2} \\
&= \left[\frac{(\zeta_k\omega_k)^2}{\omega_{dk}} + \omega_{dk}\right] e^{-\zeta_k\omega_k(\tau-\tau_i)} \left[\zeta_k\omega_k \sin\omega_{dk}(\tau-\tau_i) - \omega_{dk}\cos\omega_{dk}(\tau-\tau_i)\right] T_m(\tau_i) \\
&- \frac{e^{-\zeta_k\omega_k(\tau-\tau_i)}}{\omega_{dk}} \left\{ \begin{array}{l} \left[\zeta_k\omega_k\omega_{dk} + (\zeta_k\omega_k)^2\right]\cos\omega_{dk}(\tau-\tau_i) \\ + \left[\zeta_k\omega_k + (\omega_{dk})^2\right]\sin\omega_{dk}(\tau-\tau_i) \end{array} \right\} \frac{dT_m(\tau_i)}{d\tau} + \tilde{F}_{mn}(\tau) \\
&- \frac{1}{\omega_{dk}} \int_{\tau_i}^{\tau} e^{-\zeta_k\omega_k(\tau-\chi)} \left\{ \begin{array}{l} \left[\zeta_k\omega_k\omega_{dk} + (\zeta_k\omega_k)^2\right]\cos\omega_{dk}(\tau-\chi) \\ + \left[\zeta_k\omega_k + (\omega_{dk})^2\right]\sin\omega_{dk}(\tau-\chi) \end{array} \right\} \tilde{F}_{mn}(\chi)d\chi.
\end{aligned} \tag{26}$$

where $\omega_k^2 = \left(\omega_{mn}^2 + k\right)$, $2\zeta_k\omega_k = c$ and $\omega_{dk} = \omega_k\sqrt{1-\zeta_k^2}$

In summary, if parameter λ of Eq. (21) in the domain $\{\tau_i, \tau_{i+1}\}$ satisfies the minimum error condition (22), accurate time functions $\left\{T_{mn}, dT_{mn}/d\tau, d^2T_{mn}/d\tau^2\right\}$ can be obtained via Eq. (26). Substituting these back into Eq. (24) will determine the displacement in the domain $\{\tau_i, \tau_{i+1}\}$. Moreover, the overall dynamic behavior can be determined step by step. When the time subinterval $\Delta\tau$ approaches to zero, the overall accurate solution is successfully determined [Lin, 201].

Table 1: Convergence of the proposed method [$\bar{g} = 0.1\zeta_c = 0.5$, r= 1, $c = c_c = k = k_c$=0].

number of time subintervals	$w(0.5,0.5,\tau(\xi_c=1))/w_s(0.5,0.5)$					
	$m_c = 0.1, \quad \xi_c = 0.5\tau$			$m_c = 0.2, \quad \xi_c = \tau$		
	number of terms$(M\times N)$			number of terms$(M\times N)$		
	(6×6)	(8×8)	(10×10)	(10×10)	(14×14)	(18×18)
1000	0.0693	0.0693	0.0686	0.0632	0.0614	0.0613
2000	0.0692	0.0690	0.0686	0.0630	0.0610	0.0608
3000	0.0692	0.0690	0.0686	0.0630	0.0610	0.0609
4000	0.0691	0.0690	0.0686	0.0630	0.0610	0.0609
5000	0.0691	0.0690	0.0686	0.0630	0.0610	0.0609

Without the loss of generality, assume a concentrated mass moving from $x = 0$ to $x = L_1$with constant speed $d\xi_c/d\tau = v$. Table 1 verifies the effect of the number of time subintervals and the number of terms $(M\times N)$ of Eq. 24) on the numerical result of the response ratio $w(0.5,0.5,\tau(\xi_c=1))/w_s(0.5,0.5)$where $w(0.5,0.5,\tau(\xi_c=1))$is the dynamic displacement at ξg ζg 0.5 when the concentrated mass moves to the position $\xi_c = 1$ $w_s(0.5,0.5)$ is the static displacement

at the center of plate, ξg ζg 0.5, subjected to the same concentrated weight at $\xi_c = \zeta_c = 0.5$ Szilard [1974] presented the displacement of a s-s-s-s plate subjected to a concentrated load, shown in Figure 1b, as

$$w_s(\xi,\zeta) = \frac{4}{\pi^4} m_c \bar{g} \sum_{m=1}^{\infty} \sum_{n=1}^{\infty} \frac{\sin(m\pi\xi_c)\sin(n\pi r\zeta_c)}{\left[m^2 + (nr)^2\right]^2} \sin(m\pi\xi)\sin(n\pi r\zeta) \tag{27}$$

The numerical result determined by the proposed method converges very rapidly. Even when the number of subintervals is only one thousand, the difference between the present displacement and the converged displacement is less than 0.29% . However, when the mass ratio and the moving speed are increased, more modes are required for the accurate results.

Table 2: Comparison of dynamic amplification factors, $w_{\max}(0.5,0.5,\tau)/w_s(0.5,0.5)$, of a simply supported 2(m) $\times$ 2(m) $\times$ 17(cm) aluminum plate by the proposed method compared to the method of Nikkhoo and Rofooei [2012] when the concentrated mass moves at a constant speed along a trajectory parallel to the plate edge, i.e., $\zeta_c(\tau) = 0.5$, from $\xi_c = 0$ to $\xi_c = 1$. [E= 731 $\times$ 10^{10} pa, ρ = 2700 kgm^{-3}, μg= 0.33$c = c_c = k = k_c$=0, r= 1.0, and the moving speed $V = \beta v'$, $v' = 2L_1/T_1$ in which T_1 is the first period of vibration of the plate].

m_c	$\beta = V/v'$	$w_{\max}(0.5,0.5,\tau)/w_s(0.5,0.5)$	
		proposed	[Nikkhoo and Rofooi, 2012]
0.15	0.2	1.11	1.12
	0.3	1.47	1.47
	0.4	1.61	1.62
	0.5	1.63	1.64
	0.6	1.70	1.72
0.30	0.2	1.22	1.22
	0.3	1.54	1.54
	0.4	1.64	1.65
	0.5	1.73(*)	1.89
	0.6	1.83(*)	2.03
*: separation			

Table 2 demonstrates the comparison of dynamic amplification factors (DAF), $w_{\max}(0.5,0.5,\tau)/w_s(0.5,0.5)$, of a simply supported 2(m) $\times$ 2(m) $\times$ 17(cm) aluminum plate by the presented method versus the results from Nikkhoo and Rofooei [34] when the concentrated mass moves at a constant speed along a parallel trajectory

to the plate edge, i.e., $\zeta_c(\tau) = 0.5$, from $\xi_c = 0$ to $\xi_c = 1$. The dynamic amplification factor is the ratio of the plate's absolute maximum dynamic deflection to its maximum static response at the plate's center point. If the mass ratio m_c and the moving speed v are small, the results determined by the presented method and Nikkhoo and Rofooei [2012] are very consistent. However, for larger mass ratio m_c and the moving speed, the difference between the approaches is significant. By the presented method, the separation phenomenon is found.

2.3 Mechanism of Separation and Factors

2.3.1 Critical condition of separation

The mechanism of a vehicle separating from a plate is described in the following. If there is no guide keeping the vehicle in connection with the plate as shown in Figure 1a, the vehicle may separate from the plate when the interacting contact force f_c changes from compressive to tensional. When compressive or positive contact force f_c exists, the vehicle will move along the plate. However, when normal contact force f_c is decreased to be zero, the vehicle will separate from the plate. Therefore, the critical condition of separation is '$f_c(\tau) = 0$'.

2.3.2 Effect of parallel trajectory

Consider a concentrated mass moves at a constant speed along a parallel trajectory to the plate edge, i.e., $\zeta_c = 0.5$ and $\xi_c = v\tau$ from $\xi_c = 0$ to $\xi_c = 1$. One investigates the influence of the moving speed v and the aspect ratio (L_1/L_2) r on two dynamic responses $\{w(0.5,0.5,\tau),\ w(\xi_c,\zeta_c,\tau)\}$ where $w(0.5,0.5,\tau)$ is the dynamic displacement at the center of plate and $w(\xi_c,\zeta_c,\tau)$ is the dynamic displacement of the vehicle position. From Figure 2a when the aspect ratio r= 0.5 and moving speed v=0.5 if the coordinate of vehicle ξ_c is increased from ξ_c=0, the vibration responses are increased. When the vehicle moves to $\xi_c = 0.5$, the maximum responses $\{w_{\max}(0.5,0.5,\tau),\ w_{\max}(\xi_c,\zeta_c,\tau)\}$ occur. For v = 1.0 when the vehicle moves to $\xi_c = 0.43$, the maximum responses occur. In addition, for v = 2.0 when $\xi_c = 0.7$, the maximum response $w_{\max}(\xi_c,\zeta_c,\tau)$ occurs. However, the maximum response $w_{\max}(0.5,0.5,\tau)$ happens at $\xi_c = 0.75$. Obviously, the higher the moving speed v is, the larger the maximum responses are. Moreover, for higher speed v = 2.0, when the vehicle moves to $\xi_c = 0.9235$, the vehicle will separate from the plate. In other words, for the aspect ratio r = 0.5 if the moving speed is increased to v = 2.0 separation will occur.

Furthermore, in Figure 2b with aspect ratio r= 1 and v=2.0 when the concentrated mass moves from $\xi_c = 0$ to $\xi_c = 1$, separation will not occur. This differs to the plate with r =0.5 as shown in Figure 2a. The reason is that the plate with r=0.5 is

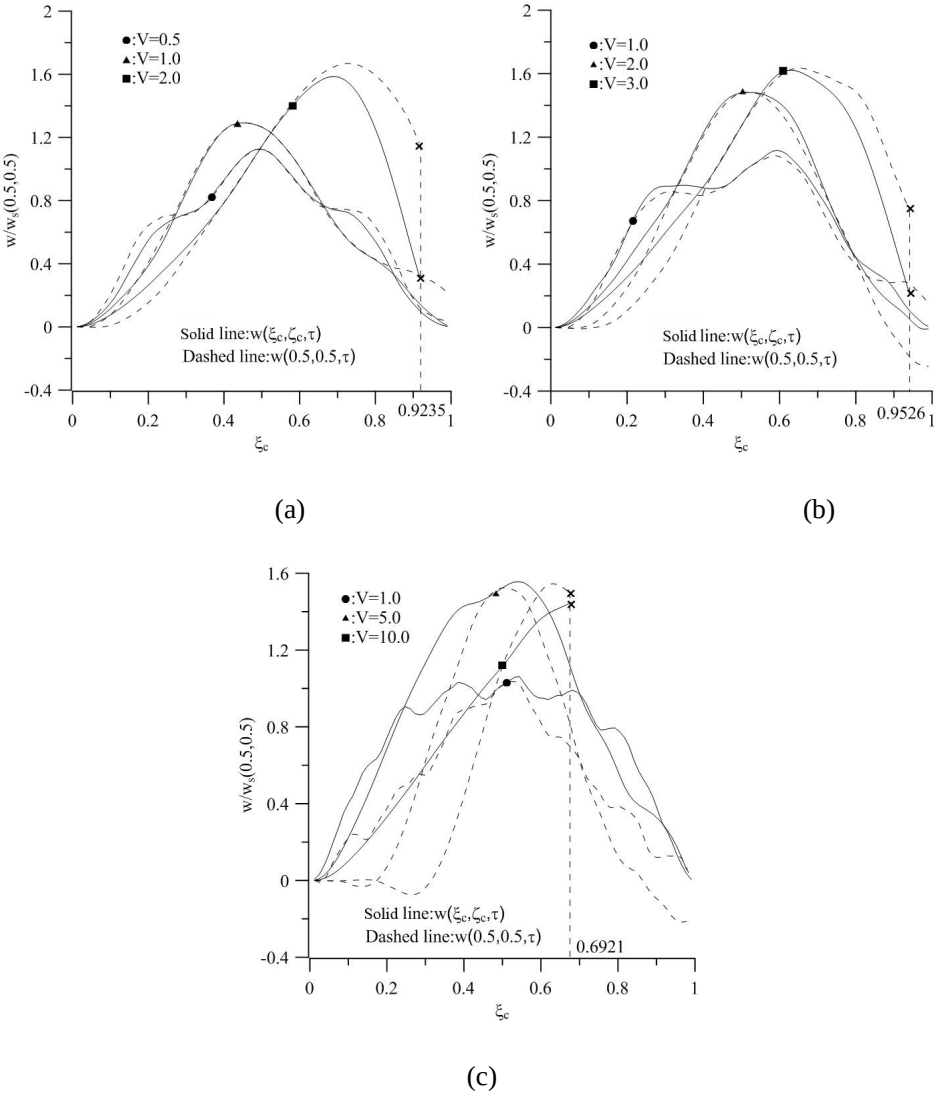

Figure 2: Influence of moving speed v and aspect ratio r on response ratio $w/w_s\,(0.5,0.5)$ when a concentrated mass moves at a constant speed along a trajectory parallel to the plate edge, i.e., $\zeta_c\,(\tau)=0.5$ from $\xi_c=0$ to $\xi_c=1$ [$m_c=0.1$, $\bar{g}=0.1$, $\xi_c\,(\tau)=v\tau$, $c=c_c=k=k_c$=0; (a): r= 0.5, (b): r= 1.0, (c): r= 2.0].

more flexible than the plate with r =1. Moreover, if moving speed v is increased to the value of 3, the vehicle will separate from the plate at $\xi_c = 0.9526$ Finally, in Figure 2c with the aspect ratio r= 2 though the moving speed is increased to v=5, separation will not occur. Finally, if the moving speed v is increased to the value of 10, the vehicle will separate from the plate at $\xi_c = 0.6921$ It is concluded from Figure 2 that the effect of moving speed v on the maximum responses is significant. When the moving speed is over the critical speed, the moving mass will separate from the plate. Also, the larger the aspect ratio r is, the higher the critical speed $v_{critical}$ is.

2.3.3 Effect of diagonal trajectory

Consider a concentrated mass moving at a constant speed along a diagonal trajectory from $\{\xi_c, \zeta_c\} = \{0,0\}$ to $\{\xi_c, \zeta_c\} = \{1, 1/r\}$, i.e., $\xi_c(\tau) = v_1\tau$, $\zeta_c(\tau) = (v_1/r)\tau$. We investigate the influence of the moving speed v_1 on two dynamic responses $\{w(0.5,0.5,\tau),\ w(\xi_c,\zeta_c,\tau)\}$ and separation From Figure 2b where v=1.0 or 2.0, the moving mass does not separate from plate However, when the speed increased to 3.0, the moving mass will separate from plate at the 0.9526 position. Figure 3 shows when v = 2 or 3 and the vehicle moves to $\xi_c = 0.9575$ or 0.8858, it will separate from the plate. Further, it is observed from Figures 2b and 3 with aspect ratio r=1 and moving speed v=2, separation will occur along a diagonal trajectory instead of a parallel to the plate edge. This demonstrates the effects of aspect ratio r and moving trajectory on critical speed are significant. A detailed investigation follows.

2.3.4 Effects of aspect ratio and mass ratio

Figure 4 demonstrates the relationship among the aspect ratio r, the concentrated mass ratio m_c and the critical speed $v_{critical}$. It shows the larger the aspect ratio r is, the higher the critical speed $v_{critical}$. However, the larger the concentrated mass m_c is, the lower the critical speed $v_{critical}$. Moreover, if aspect ratio r is small, the critical speed of a diagonal trajectory is lower than that of a trajectory parallel to the plate edge. On the other hand, if the aspect ratio r is large, the critical speed of a diagonal trajectory is higher than that of a parallel one. At the critical aspect ratio $r_{critical}$, the critical speeds are same. Note the larger the mass m_c is, the smaller the critical aspect ratio $r_{critical}$.

2.3.5 Effect of foundation

Figure 5 demonstrates the influence of the spring and damping constants $\{k,c\}$ of foundation on the critical speed $v_{critical}$ when the concentrated mass moves at a constant speed along a trajectory parallel to the plate edge, i.e., $\zeta_c(\tau) = 0.5$, from

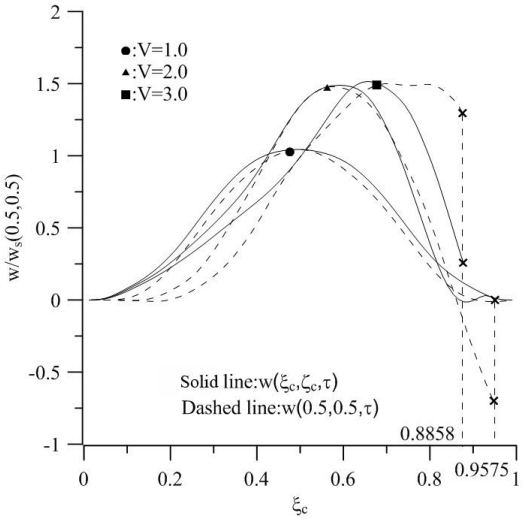

Figure 3: Influence of moving speed v on response ratio $w/w_s(0.5,0.5)$ when a concentrated mass moves at a constant speed along a diagonal trajectory from $\{\xi_c,\zeta_c\}=\{0,0\}$ to $\{\xi_c,\zeta_c\}=\{1,1\}$ [$m_c=0.1,\ \bar{g}=0.1\xi_c(\tau)=v_1\tau;\ \zeta_c(\tau)=(v_1/r)\tau$,, r= 1, $c=c_c=k=k_c$=0].

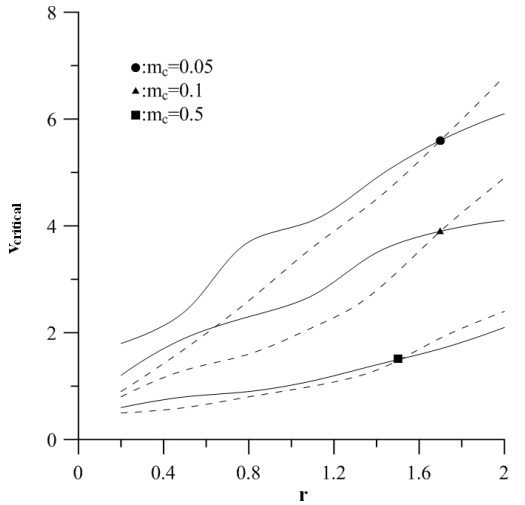

Figure 4: Influence of moving mass $m_c$and aspect ratio $r$on critical speed $v_{1,critical}$ when a concentrated mass moves at a constant speed. [$\bar{g}=0.01\quad c=c_c=k=k_c$=0; solid line: along the trajectory parallel to the plate edge, $\xi_c(\tau)=v_1\tau;\ \zeta_c(\tau)=0.5$; dashed line: along the diagonal trajectory $\xi_c(\tau)=v_1\tau;\ \zeta_c(\tau)=v_2\tau v_1/v_2=r$].

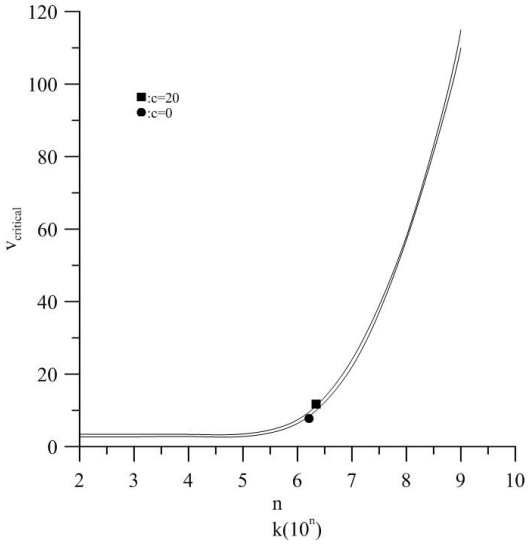

Figure 5: Influence of the spring constant k and damping coefficient$c$ on the critical speed when a concentrated mass moves at a constant speed along a trajectory parallel to the plate edge, i.e., $\zeta_c(\tau) = 0.5$ from $\xi_c = 0$ to $\xi_c = 1$ [$m_c = 0.1$, $\bar{g} = 0.1$, r=1].

$\xi_c = 0$ to $\xi_c = 1$ We find the spring constant k is smaller than the value of 10^5 and the critical speed $v_{critical}$ is almost constant. Further, the critical speed $v_{critical}$ increases greatly with the spring constant k Moreover, the larger the damping coefficients$c$, the higher the critical speed $v_{critical}$.

2.3.6 *Effect of nonconstant moving speed*

We investigate the effects of three different movements on the dynamic response ratio $w(\xi_c, \zeta_c, \tau)/w_s(0.5, 0.5)$ when the concentrated mass moves along a parallel trajectory to the plate edge and the required time from $\xi_c = 0$ to $\xi_c = 1$, is 'T'. The three movements are described as the following:

1. The first moving speed is constant, $d\xi_c/d\tau = v_0$. The corresponding position of the vehicle is $\xi_c(\tau) = v_0\tau$ and the required time period to cross the plate from $\xi_c = 0$ to $\xi_c = 1$, is $T = 1/v_0$.

2. The second moving speed is $d\xi_c/d\tau = v_{s0}[1 - \sin(\pi\tau/T)]$. The corresponding position of vehicle is $\xi_c(\tau) = v_{s0}[\tau + (T/\pi)(\cos(\pi\tau/T) - 1)]$. The corresponding parameter $v_{s0} = 1/[T(1 - 2/\pi)]$

3. The third moving speed is $d\xi_c/d\tau = \bar{v}_{s0}\sin(\pi\tau/T)$. The corresponding position of vehicle is $\xi_c(\tau) = \bar{v}_{s0}(T/\pi)[1-\cos(\pi\tau/T)]$. The corresponding parameter $\bar{v}_{s0} = \pi/2T$.

From Figure 6a with T=1 the vibration response of the third movement is the smoothest and that of the second movement is the worst. For the second movement when the vehicle moves to $\xi_c = 0.9593$, the vehicle will separate from the plate. In Figure 6b with T= 0.5 the vibration response of the second movement is the worst. When the vehicle moves to $\xi_c = 0.9868$, it will separate from the plate. This shows that if the moving speed $d\xi_c/d\tau = \bar{v}_{s0}\sin(\pi\tau/T)$, the vibration response can be significantly suppressed.

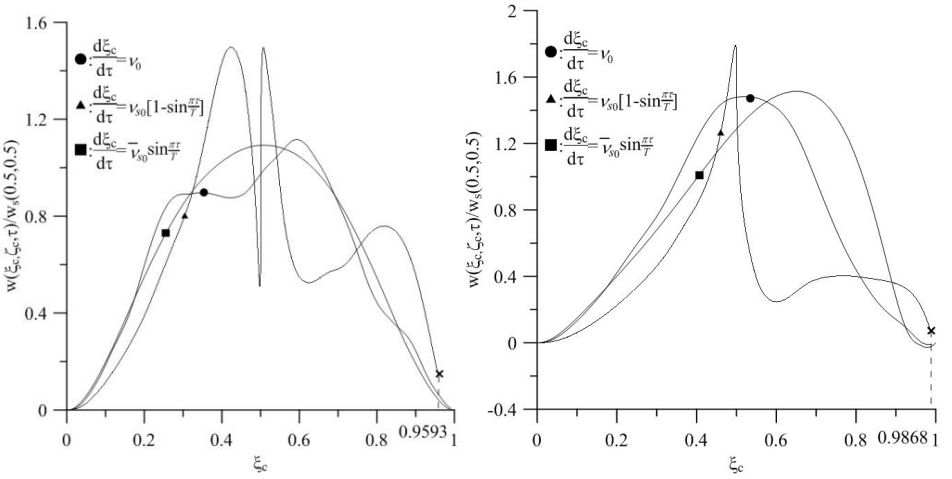

(a) (b)

Figure 6: Influence of the different movements $d\xi_c/d\tau$by the response ratio $w(\xi_c,\zeta_c,\tau)/w_s(0.5,0.5)$ when a concentrated mass moves at a constant speed along a trajectory parallel to the plate edge, i.e., $\zeta_c(\tau) = 0.5$ from $\xi_c = 0$ to $\xi_c = 1$. [$m_c = 0.1$, $\bar{g} = 0.1$, $c = c_c = k = k_c$=0, r=1 $v_{s0} = 1/[T(1-2/\pi)]$ $\bar{v}_{s0} = \pi/2T$; (a) T=1/v=1, (b): T=1/v =0.5].

3 Active Control of moving mass

Based on the above facts, there exists the phenomenon of separation and significant vibration response when there is no active control. For suppressing vibration and preventing separation the following active control law is presented.

3.1 Governing Equation and Boundary Conditions

Consider a scanning device is supported by spring and damper and moving on a plate. This can be expressed as a mass-spring-damper model moving on a plate as shown in Figure 1b. In addition to the x-y movement in the horizontal plane, z-direction movement is considered. In other words, the supporting displacement η_c is time-dependent. The dimensionless governing equation is the same as Eq. (12a) excepting the contact force:

$$f_c = \left[m_c \left(\bar{g} - \frac{d^2 w_c}{d\tau^2} \right) - c_c \left(\frac{dw_c}{d\tau} - \frac{d\eta_c}{d\tau} \right) - k_c \left(w_c - \eta_c \right) \right] \delta \left(\xi - \xi_c \right) \delta \left(\zeta - \zeta_c \right). \tag{28}$$

The associated boundary conditions are the same as Eqs. (13-2). This model is applied to simulate the system of a device scanning a plate.

3.2 Solution method

In a similar approach, the time variable t is divided into n sections and the dynamic performance of the system is derived step by step. The contact force is approximated by

$$f_c \approx \tilde{f}_c \left(\xi, \zeta, \tau \right) = \left[m_c \left(\bar{g} - \frac{d^2 \tilde{w}_c}{d\tau^2} \right) - c_c \left(\frac{d\tilde{w}_c}{d\tau} - \frac{d\eta_c}{d\tau} \right) - k_c \left(\tilde{w}_c - \eta_c \right) \right] \tag{29}$$

where

$$\frac{d^2 w_c}{d\tau^2} \approx \frac{d^2 \tilde{w}_c}{d\tau^2} = \left[\frac{d^2 w_c \left(\tau_i \right)}{d\tau^2} + \lambda \left(\tau - \tau_i \right) \right], \tag{30a}$$

$$\frac{dw_c \left(\tau \right)}{d\tau} \approx \frac{d\tilde{w}_c \left(\tau \right)}{d\tau} = \frac{dw_c \left(\tau_i \right)}{d\tau} + \left(\frac{d^2 w_c \left(\tau_i \right)}{d\tau^2} - \lambda \tau_i \right) \left(\tau - \tau_i \right) + \frac{1}{2} \lambda \left(\tau^2 - \tau_i^2 \right), \tag{30b}$$

and

$$\begin{aligned} w_c \left(\tau \right) \approx \tilde{w}_c \left(\tau \right) = & w_c \left(\tau_i \right) + \left[\frac{dw_c \left(\tau_i \right)}{d\tau} - \tau_i \left(\frac{d^2 w_c \left(\tau_i \right)}{d\tau^2} - \lambda \tau_i \right) - \frac{1}{2} \lambda \tau_i^2 \right] \left(\tau - \tau_i \right) \\ & + \frac{1}{2} \left(\frac{d^2 w_c \left(\tau_i \right)}{d\tau^2} - \lambda \tau_i \right) \left(\tau^2 - \tau_i^2 \right) + \frac{1}{6} \lambda \left(\tau^3 - \tau_i^3 \right). \end{aligned}$$

(30c)

The dynamic solution and the forcing term of Eq. (23) are the same as Eq. (24) where

$$\tilde{F}_{mn}(\tau)=4\left[m_c\left(\bar{g}-\frac{d^2\tilde{w}_c}{d\tau^2}\right)-c_c\left(\frac{d\tilde{w}_c}{d\tau}-\frac{d\eta_c}{d\tau}\right)-k_c\left(\tilde{w}_c-\eta_c\right)\right]\sin m\pi\xi_c(\tau)\sin n\pi r\zeta_c(\tau) \tag{31}$$

Except Eqs. (30, 31), the solution method is the same as the moving mass system.

3.3 Control Law

For suppression of vibration the following control law is assumed:

$$\frac{d\eta_c(\tau)}{d\tau}=\frac{d\eta_c(\tau_i)}{d\tau}+G\frac{d^2w_c(\tau_i)}{d\tau^2}(\tau-\tau_i)$$

and

$$\eta_c(\tau)=\eta_c(\tau_i)+\frac{d\eta_c(\tau_i)}{d\tau}(\tau-\tau_i)+G\frac{d^2w_c(\tau_i)}{d\tau^2}\left[\frac{1}{2}\left(\tau^2-\tau_i^2\right)-\tau_i(\tau-\tau_i)\right]. \tag{32}$$

The velocity of scanner foundation $d\eta_c(\tau)/d\tau$ is proportional to the acceleration of the scanner device position. If the control parameter G is positive, velocity is increased with acceleration. Conversely, if parameter G is negative, velocity is decreased with acceleration. The scanner device moves at a constant speed along a trajectory parallel to the plate edge from $\xi_c=0$ to $\xi_c=1$ The effect of control parameter G on the dynamic response is investigated and plotted in Figure 7. It shows when the control parameter $G=-2000$, the vibration of the scanner device approaches zero demonstrating this control law is effective. Further, Figure 8 demonstrates the influence of the spring constant k_c and the damping coefficient c_c on the suppression of vibration. It is found that the effect of the spring constant k_c on the suppression of vibration displacement is significant, but that of the damping coefficient c_c negligible.

4 Applicability of the moving-load model

This theory refers to the Appendix (moving load model). It is well known that separation cannot be studied using the moving load model. Figure 9 compares the vibration displacements at the moving position in the moving-load and moving-mass models. From Figure 9a and 9b with aspect ratio r=1, the displacements $w(\xi_c,\zeta_c,\tau)$ in the two models are almost consistent at the initial part of trajectory.

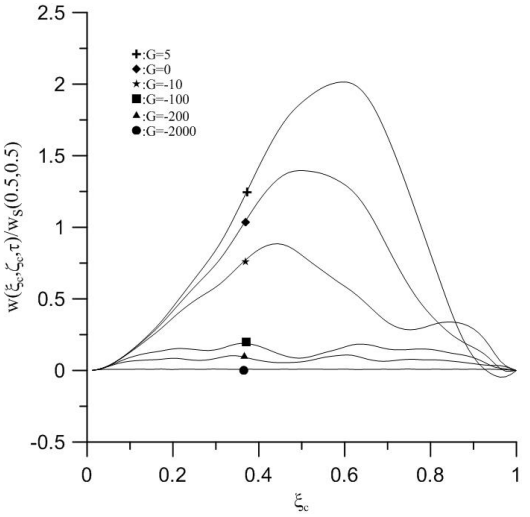

Figure 7: Influence of control gain G on the suppression of vibration when a concentrated mass moves at a constant speed along a trajectory parallel to the plate edge, i.e., $\zeta_c(\tau) = 0.5$ from $\xi_c = 0$ to $\xi_c = 1$. [$c_c = 5k_c = 5$,,$c = k = 0$, $m_c = 0.1\bar{g} = 0.1$,,$\xi_c(\tau) = 2\tau$ r= 1].

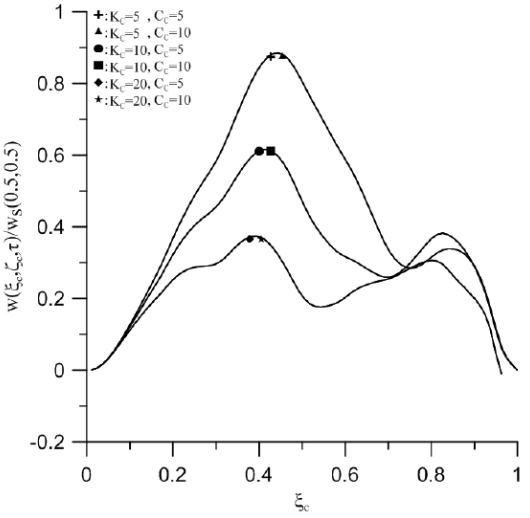

Figure 8: Influence of the spring constant k_c and the damping coefficient c_c on the suppression of vibration when a concentrated mass moves at a constant speed along a trajectory parallel to the plate edge, i.e., $\zeta_c(\tau) = 0.5$, from $\xi_c = 0$ to $\xi_c = 1$. [$G = -10$, $c = k = 0 m_c = 0.1$,,$\bar{g} = 0.1\xi_c(\tau) = 2\tau$,, r= 1].

But the difference gradually increases with the coordinates of the vehicle, ξ_c. For r=1 or 2, when the vehicle moves with the speed of v = 3 or 10, it will separate from the plate at ξ_c =0.9526 or 0.6921, respectively Note, the larger the aspect ratio r and the moving speed v are, the greater their difference between the displacements $w(\xi_c, \zeta_c, \tau)$ of the two models. This shows the moving mass problem may be accurately approximated by the moving load model only when the moving speed v is very slow and at the initial part of the trajectory.

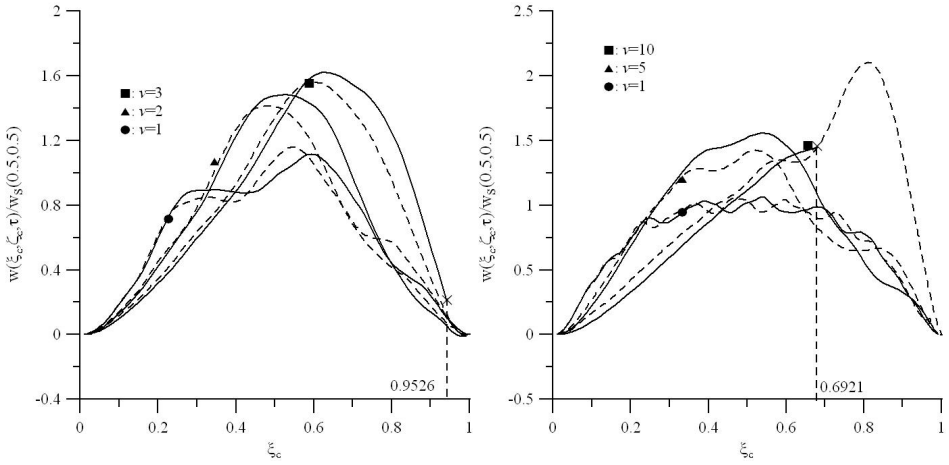

Figure 9: Influence of moving speed v and aspect ratio r on the response ratio $w/w_s(0.5, 0.5)$ when a concentrated mass moves at a constant speed v along a trajectory parallel to the plate edge, i.e., $\zeta_c(\tau) = 0.5$, from $\xi_c = 0$ to $\xi_c = 1$ [$c = c_c = k = k_c$=0, $m_c = 0.1$, $\bar{g} = 0.1$, $\xi_c(\tau) = v\tau$; (a): r= 1, (b): r= 2; solid line: moving mass model; dashed line: moving load model].

5 Conclusion

The moving mass problem may be accurately approximated by the moving load model with constraints of low moving speed v and only at the initial part of the trajectory. Separation cannot be studied by using the moving-load model. An effective control methodology for the suppression of vibration of a device moving on a plate is proposed in this work and the effects of several parameters on the separation and the vibration control of system are discovered as follows:

1. For a diagonal or parallel trajectory the larger the aspect ratio r is, the higher the critical speed $v_{critical}$.

2. For a diagonal or parallel trajectory the larger the concentrated mass m_c is, the lower the critical speed $v_{critical}$.

3. If the aspect ratio r is small, the critical speed of a diagonal trajectory is lower than that of a parallel one. But if the aspect ratio r is large, the critical speed of a diagonal trajectory is higher compared to a parallel trajectory.

4. If the spring constant k of the Winkler foundation is smaller than the value of 10^5, critical speed $v_{critical}$ is almost constant. At the same time, the larger the damping coefficients$c$ is, the higher the critical speed $v_{critical}$.

5. If varying moving speed such as $d\xi_c/d\tau = \bar{v}_{s0}\sin(\pi\tau/T)$ is considered, vibration response can be significantly suppressed.

6. The effect of the spring constant k_c on the suppression of vibration displacement is significant but the effect of the damping coefficient c_c is negligible.

References

Akin, J. E.; Mofid, M. (1989): Numerical solution for response of beams with moving mass. *Journal of Structural Engineering*, vol. 115, no. 1, pp. 120–31.

Amiri, J. V.; Nikkhoo, A.; Davoodi, M. R.; Hassanabadi, M. E. (2013): Vibration analysis of a Mindlin elastic plate under a moving mass excitation by eigenfunction expansion method. *Thin-Walled Structures*, vol. 62, pp. 53-64.

Au, F. T. K.; Wang, M. F. (2005): Sound radiation from forced vibration of rectangular orthotropic plates under moving loads. *Journal of Sound and Vibration*, vol. 281, pp. 1057–1075.

Beskou, N. D.; Theodorakopoulos, D. D. (2011): Dynamic effects of moving loads on road pavements: A review. *Soil Dynamics and Earthquake Engineering*, vol. 31, pp. 547567.

Eftekhari, S. A.; Jafari, A. A. (2012): Vibration of an initially stressed rectangular plate due to an accelerated traveling mass. *Scientia Iranica A*, vol. 19, no. 5, pp. 1195-1213.

Elliott, M. T.; Ma, X.; Brett, P. N. (2007): Tracking the position of an unknown moving load along a plate using the distributive sensing method. *Sensors and Actuators A*, vol. 138, pp. 28–36.

Esen, I. (2013): A new finite element for transverse vibration of rectangular thin plates under a moving mass. *Finite Elements in Analysis and Design*, vol. 66, pp. 26–35

Gbadeyan, J. A.; Oni, S. T. (1995): Dynamic behaviour of beams and rectangular plates under moving loads. *Journal of Sound and Vibrations*, vol. 182, no. 5, pp. 677–695.

Gbadeyan, J. A.; Dada, M. S. (2006): Dynamic response of a Mindlin elastic rectangular plate under a distributed moving mass. *International Journal of Mechanical Sciences*, vol. 48, pp. 323–340.

Ghafoori, E.; Asghari, M. (2010): Dynamic analysis of laminated composite plates traversed by a moving mass based on a first-order theory. *Composite Structures*, vol. 92, no. 8, pp. 1865–1876.

Huang, M. H.; Thambiratnam, D. P. (2001): Deflection response of plate on Winkler foundation to moving accelerated loads. *Engineering Structures*, vol. 23, no. 9, pp. 1134–1141.

Huang, F. Y.; Mote Jr. C. D. (1996): Mathematical analysis of stability of spinning disc under rotating, arbitrary large damping forces. *ASME Journal of Vibration and Acoustics*, vol. 118, pp. 657–662.

Kim, S. M. (2004): Buckling and vibration of a plate on elastic foundation subjected to in-plane compression and moving loads. *International Journal of Solids and Structures*, vol. 41, no. 20, pp. 5647–5661.

Law, S. S.; Bu, J. Q.; Zhu, X. Q.; Chan S. L. (2007): Moving load identification on a simply supported orthotropic plate. *International Journal of Mechanical Sciences*, vol. 49, pp. 1262–1275.

Lee, S. Y.; Yhim, S. S. (2004): Dynamic analysis of composite plates subjected to multi-moving loads based on a third order theory. *International Journal of Solids and Structures*, vol. 41, pp. 4457–4472.

Lin, S. M. (2009a): Vibration suppression of a moving beam subjected to an active-control electrostatic force. *CMES Computer Modeling in Engineering and Science,* vol. 43, no. 1, pp. 73-90.

Lin, S. M. (2009b): Vibrations of in-plane non-constant inward and outward rotating beams. *CMES Computer Modeling in Engineering and Science,* vol. 52, no. 1, pp. 105-124.

Lin, S.M. (2010): Nonlinear vibration of the double-beams assembly subjected to a.c. electrostatic force. *CMES Computer Modeling in Engineering and Science,* vol. 60, no. 1, pp. 95-114.

Lin, S.M. (2011): In-plane vibration of a beam picking and placing a mass along

arbitrary curved tracking. *CMES Computer Modeling in Engineering and Science,* vol. 72, no. 1, pp. 17-35.

Malekzadeh, P.; Fiouz, A. R.; Razi, H. (2009): Three-dimensional dynamic analysis of laminated composite plates subjected to moving load. *Composite Structures*, vol. 90, no. 2, pp. 105–114.

Malekzadeh, P.; Haghighi, M. R. G.; Gholami, M. (2010): Dynamic response of thick laminated annular sector plates subjected to moving load. *Composite Structures*, vol. 92, no. 1, pp. 155–163.

Martı'nez-Rodrigo, M. D.; Museros, P. (2011): Optimal design of passive viscous dampers for controlling the resonant response of orthotropic plates under high-speed moving loads. *Journal of Sound and Vibration*, vol. 330, pp. 1328–1351.

Nikkhoo, A.; Rofooei, F. R.; Shadnam, M. R. (2007): Dynamic behavior and modal control of beams under moving mass. *Journal of Sound and Vibrations*, vol. 306, pp. 712–724.

Nikkhoo, A.; Rofooei, F. R. (2012): Parametric study of the dynamic response of thin rectangular plates traversed by a moving mass. *Acta Mechanica,* vol. 223, no. 1, pp. 15–27.

Rofooei, F. R.; Nikkhoo, A. (2009): Application of active piezoelectric patches in controlling the dynamic response of a thin rectangular plate under a moving mass. *International Journal of Solids and Structures*, vol. 46, pp. 2429–2443.

Sheng, G. G.; Wang, X. (2011): Response and control of functionally graded laminated piezoelectric shells under thermal shock and moving loadings. *Composite Structures*, vol. 93, no. 1, pp. 132–141.

Szilard, R. (1974): *Theory and analysis of plates: classical and numerical methods*. Prentice-Hall, Inc.

Wu, J. J. (2007): Vibration analyses of an inclined flat plate subjected to moving loads. *Journal of Sound and Vibration*, vol. 299, no. 12, pp. 373-387.

Wu, J. J. (2005): Dynamic analysis of a rectangular plate under a moving line load using scale beams and scaling laws. *Computers and Structures*, vol. 83, pp. 1464–1658.

Zhang, Q. M.; Wang, X. C.; Liu, H. (2011): Theoretical analysis of load-carrying characteristics of a simply supported dual-duct rectangular plate under moving loads. *Computers and Mathematics with Applications*, vol. 61, pp. 2306–2312.

Appendix: Moving load model

The geometry coordinates of the moving-load model are shown in Figure 1b. The corresponding governing equation is

$$\nabla^4 w + c\frac{\partial w}{\partial \tau} + kw + \frac{\partial^2 w}{\partial \tau^2} = f_c(\xi, \zeta, \tau), \tag{A1}$$

where $f_c(x,y,t) = p_0 \delta(\xi - \xi_c(t))\,\delta(\zeta - \zeta_c(t))$ in which $p_0 = PL_1^2/DL_2$. Because the force is independent to displacement, the phenomenon of separation must not occur. This implies that the moving-load model is not applicable for the separation of the system.

Because load f_c is independent to displacement w, the dynamic solution and the forcing term of Eq. (A1) can be expressed as

$$w = \sum_{m=1}^{\infty}\sum_{n=1}^{\infty} T_{mn}(\tau)\sin m\pi\xi \sin n\pi r\zeta, \tag{A2}$$

and

$$f_c(\xi, \zeta, \tau) = \sum_{m=1}^{\infty}\sum_{n=1}^{\infty} F_{mn}(\tau)\sin m\pi\xi \sin n\pi r\zeta, \tag{A3}$$

where $F_{mn}(\tau) = 4p_0 \sin m\pi\xi_c \sin n\pi r\zeta_c$.

Substituting Eq. (A2) into the governing equation Eq. (A1) results in

$$\frac{d^2 T_{mn}}{d\tau^2} + c\frac{dT_{mn}}{d\tau} + \left(\omega_{mn}^2 + k\right) T_{mn} = F_{mn}(\tau) \tag{A4}$$

The solutions of Eq. (A4) are derived as follows:

$$\begin{aligned} T_{mn}(\tau) = {} & e^{-\zeta_k \omega_k \tau}\left[\cos\omega_{dk}\tau + \tfrac{\zeta_k\omega_k}{\omega_{dk}}\sin\omega_{dk}\tau\right] T_{mn}(0) + \tfrac{1}{\omega_{dk}} e^{-\zeta_k\omega_k\tau}\sin\omega_{dk}\tau \tfrac{dT_{mn}(0)}{d\tau} \\ & + \tfrac{1}{\omega_{dk}}\int_0^\tau e^{-\zeta_k\omega_k(\tau-\chi)}\sin\omega_{dk}(\tau-\chi) F_{mn}(\chi) d\chi \end{aligned} \tag{A5}$$

Substituting Eq. (A5) back into Eq. (A2) results in the analytical solution.